Sensing the dissociation of a polymeric enzyme by means of an engineered intrinsic probe

ARTICLE *in* PROTEINS STRUCTURE FUNCTION AND BIOINFORMATICS · APRIL 2011

Impact Factor: 2.63 · DOI: 10.1002/prot.22945 · Source: PubMed

7 AUTHORS, INCLUDING:

Patricio Craig
University of Buenos Aires
24 PUBLICATIONS **268** CITATIONS
SEE PROFILE

Hernan R Bonomi
Fundación Instituto Leloir
13 PUBLICATIONS **110** CITATIONS
SEE PROFILE

PROTEINS
STRUCTURE ■ FUNCTION ■ BIOINFORMATICS

Sensing the dissociation of a polymeric enzyme by means of an engineered intrinsic probe

N. Ainciart, V. Zylberman, P.O. Craig, D. Nygaard, H.R. Bonomi, A.A. Cauerhff, and F.A. Goldbaum*

Fundación Instituto Leloir-IIBBA-CONICET, Av. Patricias Argentinas 435 Buenos Aires (1405), Argentina

ABSTRACT

One of the most remarkable characteristics of Brucella lumazine synthase (BLS) is its versatility to undergo reversible dissociation and reassociation as a polymeric scaffold. We have proposed a mechanism of dissociation and unfolding of BLS. Using static light scattering (SLS) analysis, we were able to demonstrate that the decameric assembly dissociates into two different conditions [pH 5 or 2*M* guanidinium chloride (GdnHCl) pH 7] forming stable folded pentamers. The transition from folded pentamers to unfolded monomers by GdnHCl denaturation is highly cooperative and can be measured by different spectroscopic techniques. In this work, we show the successful insertion of an intrinsic probe to study in more detail the equilibria described in previous publications. For that purpose, we performed single-point mutations of Phe residues 121 and 127, located at the pentamer–pentamer and monomer–monomer interface, respectively, to Trp residues. These mutations produced only a marginal perturbation of the BLS structure. We analyzed the unfolding and stability of the mutants through different techniques: far-and near-UV CD, SLS, dynamic light scattering, and fluorescence spectroscopy. The introduced intrinsic probe could be used to gain insights into the detailed folding and assembly mechanism of this protein.

Proteins 2011; 79:1079–1088.

Key words: homooligomeric assembly; tryptophan probe; lumazine synthase; stability.

INTRODUCTION

The enzyme lumazine synthase catalyzes the penultimate step in the biosynthesis of riboflavin in bacteria, fungi, and plants.[1–4] In all studied species, the enzyme folds as a tioredoxinlike domain of 18 kDa that associates as a highly intertwined C5-symmetry homopentameric structure. Notably, this family shows remarkable quaternary structure divergence: most of the species harbor pentameric lumazine synthases[5–7] or, alternatively, particles built from 12 pentamers arranged as icosahedral forms.[1,8–10] In a previous work[11] we described that *Brucella spp.* lumazine synthase (BLS) presents a 180 kDa decameric form not previously described. BLS folds as a remarkably stable dimer of pentamers and presents a very high thermal and chemical stability.[11] Besides, BLS is very immunogenic, being a very interesting platform for engineering of new type of immunogens. We have used BLS for multiple antigenic displays of peptides and protein domains for vaccine design.[12–18]

One of the most remarkable characteristics of BLS is its capacity to reversible undergo dissociation and reassociation as a polymeric scaffold. We have proposed a mechanism of dissociation and unfolding of BLS. The decameric assembly dissociates into two different conditions to stable folded pentamers, with an estimated ΔG of 90 $\pm$ 20 kJ/mol per decamer. BLS shifts from a decameric to a pentameric quaternary state at acidic pH, maintaining the overall folding of the protein. The pH effect on dissociation would be explained by the high density of histidines at the pentamer–pentamer interface. Imidazole ring of His residues become protonated at pH levels below 6.0,[19–21] thus producing charge repulsion and loss of a large number of contacts resulting in the dissociation of the decamer. In contrast, this mild protonation does not disturb the stability of the monomer–monomer interface, because ~35% of the accessible surface area (ASA) of each monomeric polypeptide is engaged in intrapentameric hydrophobic contacts.[11,22,23] The addition of guanidinium chloride (GdnHCl) first produces the dissociation of folded pentamers (at 2.0–2.2*M* range) and then the highly cooperative pentamer unfolding (at guanidinium concentrations of 3.0*M*), with a value of ΔG of 300–330 kJ/mol pentamer. This high value of free energy would be the product of the tight and intertwined nature of the monomer–monomer interface, stabilized by a large number of van der Waals contacts. On the other hand, BLS is very stable to thermal denaturation, showing a melting temperature of

N. Ainciart and V. Zylberman contributed equally to this work.
*Correspondence to: Fernando Goldbaum, Av. Patricias Argentinas 435 Buenos Aires (1405) Argentina.
E-mail: fgoldbaum@leloir.org.ar
Received 20 September 2010; Revised 29 October 2010; Accepted 7 November 2010
Published online 19 November 2010 in Wiley Online Library (wileyonlinelibrary.com). DOI: 10.1002/prot.22945

88°C ± 2°C, whereas the pentameric intermediate denatures at 70°C, again showing the remarkable stability of the assembly.[9,11]

In this work, we show the successful insertion of an intrinsic probe to characterize the intermediate pentamers and the associated equilibrium. We used site-direct mutagenesis to introduce Trp residues at the interface between pentamers. We show that the mutation of Phe 121 and 127 to Trp produces only a marginal perturbation of the BLS structure. We analyzed the folding, unfolding, and stability of the mutants through different techniques: far- and near-UV circular dichroism, static light scattering (SLS), dynamic light scattering (DLS), and fluorescence spectroscopy. Besides introducing Trp residues at the interface, we also mutated the native Trp 22 in order to avoid spectroscopic interference of this residue when fluorescence experiments were performed. Strikingly, insertion of a Trp at position 127 further stabilizes the BLS assembly and allows for a sensitive measurement of different equilibria. These characteristics will be useful for future kinetics and protein engineering studies and to establish the conditions for reversibly assembly of fusion proteins with different functionalities and generation of mixed particles.

METHODS

Structural analysis

Structural analysis of the residues forming BLS protein was performed using 1XN1 PDB entry as model.[22] The numbering of the amino acids was taking into account the PDB file; it means that the mutated Phe was at positions 121 and 130 in sequence corresponding to Phe 121 and 127, respectively. Measurement of atomic contact distances was carried on with CSU server (http://ligin.weizmann.ac.il/cgi-bin/lpccsu/LpcCsu.cgi)[24] and using a cut off of 5.0 Å. The chosen criteria to evaluate clusters of aromatic π-stacking interaction were taken from McGaughey et al.[25] Aromatic residues pairs were considered forming aromatic π-stacking with different orientations if their $R_{clo} < 4.5$ Å and/or $R_{cen} < 7.5$Å. R_{clo} is defined as the closer distance between two aromatic rings, and R_{cen} is defined as the ring centroid–centroid separation.

Cavities and pockets were measured using CASTp server (http://sts.bioengr.uic.edu/castp/).[26]

Cloning and site-directed mutagenesis

The *Brucella spp.* LS gene was cloned in pET11a vector (Novagen) as reported previously.[27] The single replacements of amino acids Phe 121 and Phe 127 by Trp and Trp 22 by Ala were achieved by site-directed mutagenesis of pET11a-BLS plasmid and denoted, BLS-W22A-F121W, BLS-W22A-F127W, and W22A, respectively. The method of site-direct mutagenesis was descripted by Kammann et al.[28] We used three PCR reactions. In all reactions, we used Pfu DNA polymerase (purified in "Fundacion Instituto Leloir"), the appropriated buffers (Promega), and the thermocycler (Techne). In the first PCR (PCR_1), we used the pET11a-BLS plasmid as template and the universal primer Sp6 (5′-ATTTAGGTGACACTATAG), which sequence was river down the cloned site and the oligonucleotide 5′-ATTCAGGCCCGCGCCCACGCCGACATC (synthesized by IDT, Integrated DNA Technologies). This one had a 27 oligonucleotide sequence, which is complementary with a region of BLS except the codons that code for the Ala amino acid. This PCR product was purified and used as a mega-primer in the second PCR of the method. In this reaction, we used the pET11a-BLS plasmid as template and the universal primer T7 (5′-TAATAC GACTCACTAT AGGG) as the second primer. The purified product of this reaction was used as template in third PCR. This last reaction was the objective to increase the product mass, and the primers used were T7 and Sp6. We used 30 amplification cycles: 1 min at 94°C, 1 min at 55°C, and 1 min at 72°C. Then, the third PCR product was purified, digested with *Xba I* and *BamH I* restriction enzymes (Promega), and ligated to the pET11a vector (previously treated with the same restriction enzymes).

Protein expression

The plasmids obtained as described earlier were used to transform BL21(DE3) strain *Escherichia coli*-competent cells (Stratagene, La Jolla, CA). Ampicillin-resistant colonies were grown until *A*600 = 1.0 in LB medium containing 100 μg/mL ampicillin at 37°C with agitation (300 rpm). Five milliliters of this culture were diluted to 500 mL and grown to reach an *A*600 of 1.0. At this point, the culture was induced adding 1 m*M* isopropyl-1-thio-β-D-galactopyranoside and incubated for 4 h at 37°C with agitation (300 rpm). The bacteria were centrifuged at 15,000*g* during 20 min at 4°C.

Protein purification and refolding

The proteins were successfully expressed as inclusion bodies in BL21(DE3) *E. coli*-competent cells strain as described elsewhere.[27] Briefly, inclusion bodies were solubilized in 50 m*M* Tris, 5 m*M* EDTA, and 8*M* urea pH 8.0 at room temperature overnight with agitation. The solubilized material was refolded by dialysis for 72 h against phosphate-buffered saline-containing 1 m*M* dithiothreitol (DTT). This preparation was purified in a Mono-Q column in a fast-protein liquid chromatography apparatus (Amersham Biosciences, Uppsala, Sweden) using a linear gradient of 50 m*M* Tris, 1*M* NaCl, and pH 8.5 (buffer B). The peak enriched with the desired protein was further purified on a Superdex-200 column with phosphate-buffered saline buffer, 1 m*M* DTT. The purity

of the protein samples was determined on SDS-15% (w/v) polyacrylamide gels. Purified BLS was concentrated (10 mg/ml) (Centricon, Millipore), frozen in liquid N2, and stored at 20°C.

Circular dichroism

BLS, its mutants, and control protein samples were diluted in 50 m*M* sodium phosphate, pH 7.0, and 1 m*M* DTT, with increasing concentration of denaturants (urea or GdnHCl). All experiments were performed at 25°C, and samples were incubated at least 2 h before performing CD measurements. Spectra were measured on a spectropolarimeter (JASCO J-810) using either 0.1- or 0.5-cm path length quartz cells. Unfolding was monitored by far-UV CD (260–200 nm) and expressed as the percentage of molar ellipticity at 222 nm as a function of denaturant concentration. The molar ellipticity of the protein incubated without GdnHCl was taken as 100%. For renaturation tests, proteins were first denatured in high concentration of GdnHCl (6*M*), and renaturation was induced by overnight dialysis against 50 m*M* sodium phosphate, pH 7.0, and 1 m*M* DTT. After this treatment, the CD and SLS signals typical of the native protein were recovered.

Intrinsic fluorescence measurements

Emission spectra were carried out by excitation of the samples at 295 nm, and data collection from 300 to 400 nm, using 3-nm band passes for both excitation and emission. Experiments were carried out in 50 m*M* sodium phosphate, pH 7.0, and 1 m*M* DTT in the presence of increasing concentrations of urea or GdnHCl. Samples were incubated for at least 2 h before taking fluorescence measurements. All fluorescence emission spectra were measured at 25°C on a Jasco FP-770 spectrofluorometer.

The center of mass was calculated,

$$\mathrm{CM} = \sum (\lambda_i * I_i) \Big/ \sum I_i$$

where λ_i is the wavelength and I_i is the fluorescence intensity en each wavelength λ_i.

Thermal denaturation monitored by CD

BLS, its mutants, and control protein samples were incubated in 50 m*M* sodium phosphate, 1 m*M* DTT, pH 7.0 (in the presence or absence of 2*M* GdnHCl) or in 50 m*M* buffer citrate, 1 m*M* DTT, and pH 4.5. Thermal denaturation was conducted by slowly increasing the temperature with a Peltier system (Jasco). The range of temperature scanning was 25–95°C at a speed of 4°C/min. Molar ellipticity at 220 or 280 nm was measured every 0.5°C. Fast or slow cooling back to 25°C (from 95 to 25°C at a speed of 1°C/min) did not show a recovery of ellipticity demonstrating the irreversibility of the thermal unfolding. Thus, the temperature midpoint of the thermal transition was considered as an apparent T_m.

Determination of molecular weight of BLS by static and dynamic light scattering

Static light scattering

The average molecular weight (M_w) of proteins under different conditions was determined on a Precision Detectors PD2010 light-scattering instrument tandemly connected to a high-performance liquid chromatography system and an LKB 2142 differential refractometer. In general, 20–100 µL of protein (0.3–1 mg/mL) was loaded on a Superdex 200 HR-10/30 (24 mL) or a Sephadex G-25 (1 mL) column and eluted with 50 m*M* phosphate buffer, 1 m*M* DTT under different pH, urea, GdnHCl, and NaCl conditions. The 90° light scattering and refractive index signals of the eluting material were recorded on a PC computer and analyzed with the Discovery32 software supplied by Precision Detectors. The 90° light scattering detector was calibrated using bovine serum albumin (M_w: 66.5 kDa) as a standard. Before the injection in a size exclusion chromatography column, each sample was preincubated for 1–2 h at room temperature in the elution buffer.

Dynamic light scattering

The hydrodynamic diameter of proteins was determined by dynamic light scattering (Malvern) using quartz cuvettes. Protein samples were incubated in phosphate-buffered saline for 1–2 h at room temperature and then were filtered in Ultrafree-MC Microcentrifuge filters 0.22 µm, Durapore PVDF membrane Sigma-Aldrich. The buffer was previously filtered in Nylon filters 022 µm, 47 mm, 100/Pk, OSMONICS.

Thermodynamic parameters

Thermodynamics evaluation of GdnHCl-induced unfolding of BLS was fitted to a two-step model.

$$N_{10} \overset{\mathrm{Ku1}}{\longleftrightarrow} (2)N_5 \overset{\mathrm{Ku2}}{\longleftrightarrow} 5\mathrm{U}$$

The first step (N10 ↔ 2N5) represents the dissociation of decameric BLS (N10) in two folded pentamers (N5), whereas the second step (N5 ↔ 5U) represents the concomitant dissociation and unfolding of the pentameric structure (N5) in monomeric subunits (U). Because both steps are well resolved from each other, their thermodynamic parameters were independently analyzed using the linear extrapolation method [Eq. (1)] assuming a two-state transition model for each step.[31]

$$\Delta G_U = \Delta G_{H2O} - m[D] \qquad (1)$$

where ΔG_U is the free energy of unfolding of a protein at a given denaturant concentration, ΔG_{H2O} is the free energy of unfolding in the absence of denaturant, and m the dependence of the free energy on denaturant concentration ($[D]$).

Step 1

The first step was monitored by SLS in the range of 1.5–2.2*M* GdnHCl. The concentration at equilibrium of the N_{10} and N_5 species of BLS was calculated using Eqs. (4) and (5) derived from the rearrangement of Eqs. (2) and (3),

$$\bar{M}_w = (\bar{M}_{w10} * ccN_{10} + \bar{M}_{w5} * ccN_5)/cc_T \quad (2)$$

$$cc_T = ccN_{10} + ccN_5 \quad (3)$$

$$[N_{10}] = cc_T(\bar{M}_w - \bar{M}_{w5})/(\bar{M}_{w10} - \bar{M}_{w5})\bar{M}_{w10} \quad (4)$$

$$[N_5] = (cc_T - ccN_{10})/\bar{M}_{w5} \quad (5)$$

$\overline{M}_w$ represents the average molecular weight of BLS. ccN_{10}, ccN_5, and cc_T represent the decamer, pentamer, and total protein concentration in milligrams/milliliter, respectively. $[N_{10}]$ and $[N_5]$ represent the molar concentration and $\overline{M}_{w10}$ and $\overline{M}_{w5}$ the molecular weight of the decameric (174.4 kDa) and pentameric (87.2 kDa) species of BLS, respectively.

The equilibrium constant $K_{U(1)}$ and the free energy change $\Delta G_{U(1)}$ for Step 1 are defined in Eqs. (6) and (7).

$$K_{U(1)} = [N_5]^2/[N_{10}] \quad (6)$$

$$\Delta G_{U(1)} = -RT \ln K_{U(1)} \quad (7)$$

The $\Delta G_{H2O(1)}$ and $m_{(1)}$ values [Eq. (1)] for this transition were obtained from the extrapolation to zero-denaturant concentration and from the slope of the linear regression fit of the $\Delta G_{U(1)}$ values calculated as a function of GdnHCl concentration in the range of 1.5–2.2*M*. The dissociation constant of the decameric arrangement (K_D) was estimated from the ΔG_{H2O} value of this transition using the equation, $K_D = e[-\Delta G_{H2O}/(RT)]$.

Step 2

The second step was monitored by CD and Trp fluorescence in the range of 2.4–3.5*M* GdnHCl.

$\Delta G_{H2O}(2)$ and $m_{(2)}$ values of Step 2 were obtained fitting the experimental data to Eq. (13) by a nonlinear least square fitting method. The midpoint of this transition $[D]_{50\%}$ was calculated as in Eq. (14). The derivation of Eqs. (13) and (14) [Eqs. (8–12)] are shown in the Appendix section.

$$5\left[\frac{(m_f[D]+F)-Y}{(m_f[D]+F)-(m_u[D]+U)}\right]^5 P_T^4 + \left[\frac{(m_f[D]+F)-Y}{(m_f[D]+F)-(m_u[D]+U)}-1\right] e^{(\Delta G H_2O - m(2)[D])/RT} = 0 \quad (13)$$

$$[D]_{50\%} = [RT \ln(5/16P_T^4) + \Delta G_{H2O}]/m \quad (14)$$

RESULTS AND DISCUSSION

Structural bases for the design of an intrinsic probe in BLS protein

As stated in the Introduction section, the three-dimensional structure of BLS constitutes a very tight dimer of pentamers, with 10 monomers related to one another by D5-symmetry. Figure 1 illustrates the BLS structure with special focus in the pentamer–pentamer interface. To sense the dissociation of the decamer, we introduced an intrinsic fluorescence probe at the pentamer–pentamer interface. Trp residues were chosen to mutate residues located at the interface, because they are especially suited to perform as intrinsic probes due to their particular spectroscopic properties. The selection of the positions to be mutated was carried out using the following criteria: (a) we focused in bulky Phe or Tyr residues; thus, the mutation for Trp residues would produce the most conservative change in volume, lowering the probability of structural perturbations in the tertiary and quaternary structure, (b) residues located close or at the pentamer–pentamer interface; (c) residues not exposed to the solvent in native state of BLS, that is, as dimer of pentamer, and (d) residues contacting several residues of the opposite side of the interface. In this way, a change in the spectroscopic signal is expected when those residues are exposed to solvent. Using these criteria, we found that the best candidates to be mutated by Trp were Phe 121 and 127. These two Phe are located at the pentamer–pentamer interface and participate in several contacts. Besides, their ASA values in the native structure are 3.04 and 18.26 Å^2, respectively. Phe121 presents intramonomeric contacts with His 23 (2), Ile 26 (2), Phe 80 (4) Ile 82 (6), Asp 83 (1), Pro 118 (1) His 120 (7), His 121 A (11), Glu 121 B (8), His 124 (6), His 125 (4), and Phe 128 (3). This residue does not have any contact with the other monomers of the same pentamer, but interacts with His 121 A of the opposite pentamer, forming in average three contacts. The buried surface area (BSA) of Phe 121 at the pentamer–pentamer interface is 3.30 Å^2.

Phe 127 exhibits intramonomeric contacts with Glu 123 (2), His 124 (4), Asp 126 (8), Phe 128 (13), Ala 130 (3), and His 131 (6). This residue presents in average four contacts with the adjacent monomer, contacting with Ile 86, and the BSA at monomer–monomer interface is 88.00 Å^2. At pentamer–pentamer interface, Phe 127 interacts with Glu 123 (6), His 124 (1), and Phe 127 (7) from the neighboring pentamer forming 14 contacts that add to a BSA of 71.98 Å^2.

Besides, both Phe 121 and 127 residues arrange as intramonomeric aromatic π-stacking clusters, Phe 121 interacts with His 23 (R_{clo} = 4.36 Å), Phe 80 (R_{clo} = 3.63 Å), His 124 (R_{clo} = 4.22 Å), and Phe 128 (R_{clo} =

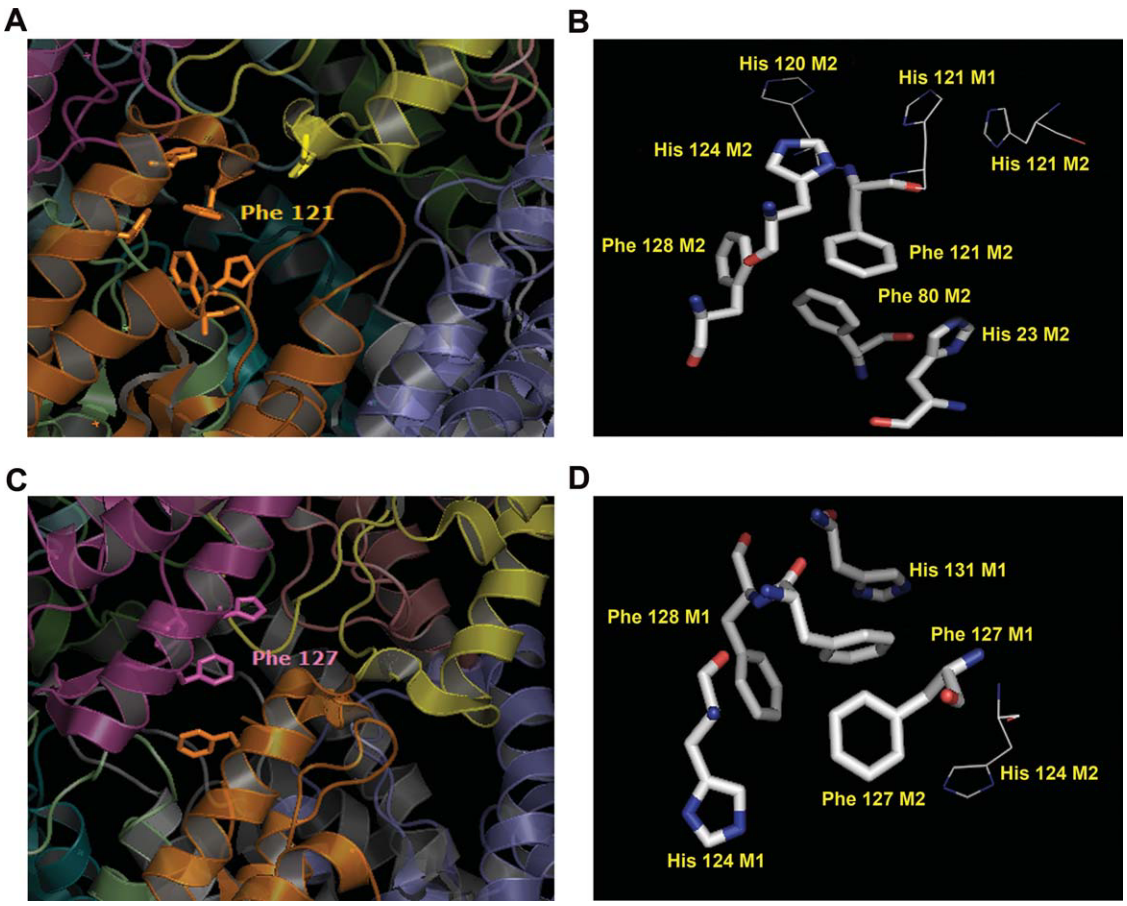

Figure 1

Aromatic contacts of Phe 121 and 127. Aromatic residues contacting Phe 121 (**A**) and Phe 127 (**C**) at the pentamer–pentamer interface are shown. The different chains of the decamer are shown as ribbons of different color to highlight the location of these Phe residues at the interface. The aromatic π-stacking cluster around Phe 121 (**B**) and Phe 127 (**D**) are shown in more detail. M1 and M2 refers to neighboring monomers at the interface.

3.70 Å) from the same chain. However, in the case of Phe 127, the aromatic π-stacking clusters are observed both in intramonomeric interactions as with Phe 128 (R_{clo} = 3.68 Å), His 131 (R_{clo} = 4.43 Å), and with His 124 (R_{clo} = 5.68 Å) as well as in pentameric–pentameric interactions as with Phe 127 (R_{clo} = 4.12 Å) from the opposite chain of the neighboring pentamer. All π-stacking interactions described present a R_{cen} lower than 7.5 Å.[25]

All other analyzed Phe and Tyr residues do not fulfill with these four criteria. We also mutated the native Trp 22 in order to avoid spectroscopic interferences of this residue when fluorescence experiments were performed. Trp 22 is exposed to the solvent with an ASA value of 130.74 Å^2, and its conformational freedom is involved in the enzymatic mechanism, being feasible to eliminate it without disturbing the stability of BLS (see below for control experiments). Trp 22 buries a surface of 24.43 Å^2 in monomer–monomer interaction, but does not participate in pentamer–pentamer interaction. Trp 22 displays intramonomeric contacts with Ala 20 (5), Arg 21 (9), His 23 (14), Ala 24 (1), Val 27 (1), Pro 54 (4), Gly 55 (2), Phe 80 (1), and seven monomer–monomer contacts with Glu 138. Trp 22 shows a π-stacking interaction with His 23 with a R_{clo} = 4.84 Å.

As any protein, BLS contains cavities in its topography. Those cavities were analyzed using the CASTp server.[26] We found that 10 of their pockets or cavities were regularly disposed inside the BLS structure, and those cavities have an average volume of 1459.90 ± 53.47 Å^3 and an average molecular surface of 888.21 Å^2. The boundaries of those repetitive cavities are formed by Phe 121 and Trp 22. Other important cavities were also found as five repetitive structures in all BLS, and this kind of cavities were limited by Phe 127, with an average volume of 328.12 Å^3 and an average molecular surface of 264.18 Å^2. Thus, Phe 121 and 127 were chosen, because they have all the structural characteristics ab initio to be replaced by Trp residues and could act as probes, including the

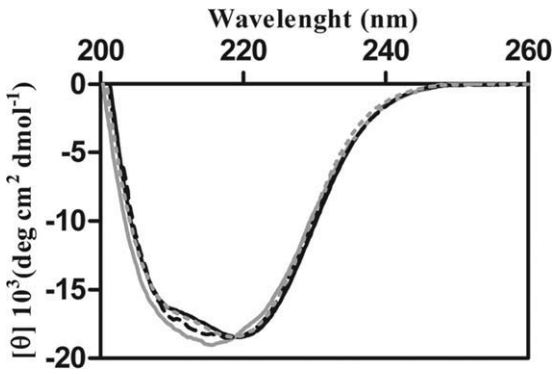

Figure 2

Far-UV CD spectra of WT BLS and mutants. The spectrum of WT BLS (solid black line), BLS-W22A-F127W (dotted gray line), BLS-W22A-F121W (dashed black line), and BLS-W22A (solid gray line) is depicted. All proteins are in 50 m*M* sodium phosphate, pH 7.0.

formation of repetitive cavities, while the other Phe or Tyr residues do not show these structural properties.

Consequently, we decided to generate the double mutants F121W-W22A and F127W-W22A. These two mutants and the control mutant W22A were efficiently produced as recombinant proteins and further analyzed as follows.

The native state of BLS mutants

The mutant proteins arrange as decamers in solution like wild-type BLS, as determined by the means of SLS and DLS. SLS experiments show that all these proteins have a molecular mass of 180 kDa in solution (data not shown). In addition, DLS analysis shows that all proteins have a hydrodynamic diameter of 11 nm (data not shown). These values correlate with a globular protein of 180 kDa.

To compare the content of secondary structure of mutants with wild-type BLS, we performed far-UV CD spectroscopy. All CD spectra were superimposable (see Fig. 2), indicating that the overall protein structure was not affected by the mutations. The small changes observed mainly in the mutant W22A (showing a minimum at 217 nm instead of at 222 nm) could be attributed to the lack of Trp residues in the protein. In effect, Vuilleumer et al.,[29] using barnase as a model protein, demonstrated that Trp residues could be the major determinants of the far-UV CD of proteins. These results of CD experiments demonstrate that the BLS folding has the capability to accommodate a Trp in the two-assayed positions, without disturbing the arrangement of the decameric assembly.

Spectroscopic characterization of the intrinsic probe

The CD spectra of proteins in the near-UV are sensitive to changes in the asymmetric environment of aromatic residues involved in the stabilization on tertiary structure. WT BLS has no signal in near-UV CD, and this fact is associated with the conformational freedom and solvent exposure of the Trp residue at position 22 [Fig. 3(A)]. However, the spectra of BLS-W22A-F121W and BLS-W22A-F127W mutants show an important signal at 280 nm, indicating that the inserted Trp residues are located in an asymmetric environment.

The intrinsic Trp fluorescence emission spectra of the proteins are shown in Figure 3(B). The emission spectrum of the WT protein shows a maximum at 358 nm, in accordance with the exposure to solvent of Trp22. The emission maxima of the mutant spectra are shifted to lower wavelengths (340 nm for BLS-W22A-F127W and 350 nm for BLS-W22A-F121W) [Fig. 3(B)]. This blue shift reflects that the introduced Trp is less exposed to the solvent than the WT BLS Trp, as can be seen in a modeled structural analysis (see Fig. 1). Thus, near-UV CD and emission fluorescence analyses confirm that the Trp residues at positions 121 and 127 are located in a more asymmetric environment (hidden to the solvent)

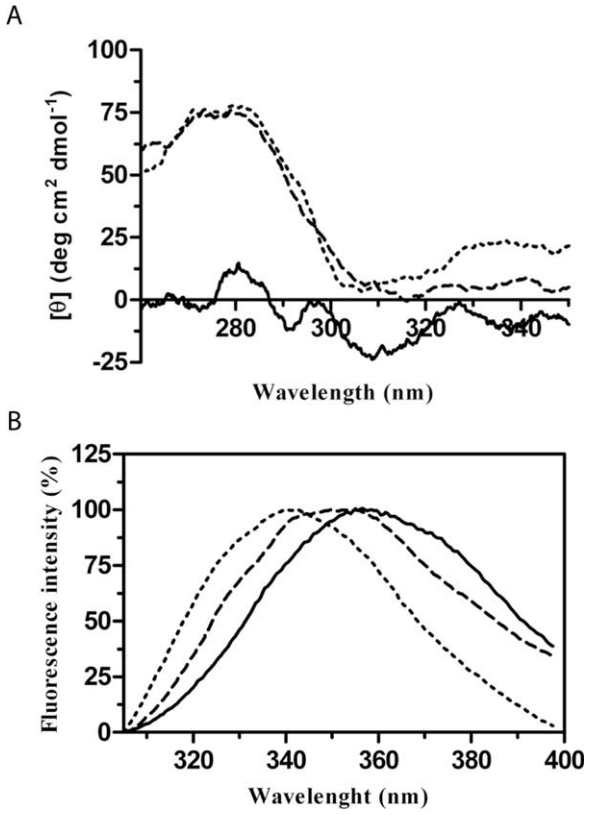

Figure 3

A: Near-UV CD spectra of WT BLS and mutants. The spectrum of WT BLS (solid line), BLS-W22A-F127W (dotted line), and BLS-W22A-F121W (dashed line) is shown. **B:** Fluorescence spectra of WT BLS and mutants. WT BLS (solid line), BLS-W22A-F127W (dotted line), and BLS-W22A-F121W (dashed line). All proteins are in 50 m*M* sodium phosphate, pH 7.0.

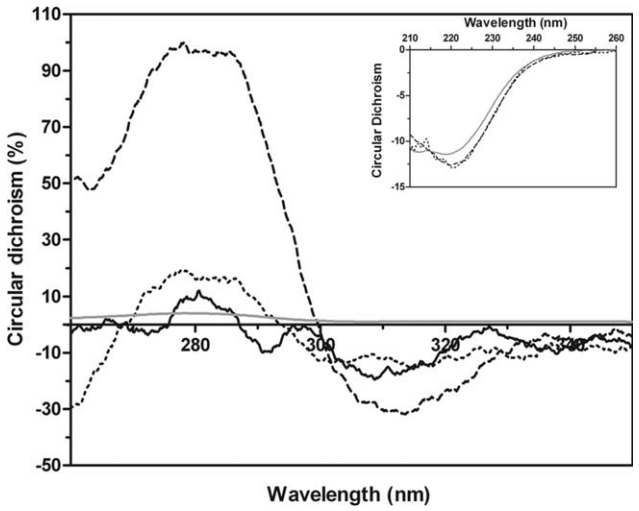

Figure 4

Circular dichroism spectra of WT BLS and mutants. Far-UV CD and near-UV CD spectra (inset) of BLS (solid black line), BLS-W22A-F127W (dashed line) in 50 m*M* sodium phosphate buffer, pH 7.0, BLS-W22A-F127W incubated in 50 m*M* acetate/citrate buffer pH 4.5 (dotted line) and BLS-W22A-F127W after incubation with 2*M* guanidinium chloride in 50 m*M* sodium phosphate buffer, pH 7.0 (solid gray line).

when compared with the Trp present in the WT protein (Trp 22). Considering that the blue shift observed for BLS-W22A-F127W was significantly more important than that observed for BLS-W22A-F121W, we decided to continue working with the first mutant.

Thermodynamic stability of BLS and BLS-W22A-F127W measured by chemical denaturation

In a previous work,[11] we have shown by SLS that BLS dissociates into pentamers at pH 4.5 or by adding low concentrations of GdnHCl. The content of secondary structure in the pentameric intermediate is identical to the existing in the decameric state. For that reason, it is not possible to detect this dissociation by means of circular dichroism in the far-UV CD. It is neither possible to detect dissociation by fluorescence or near-UV CD, due to the exposure to solvent of the native Trp22. The introduction of an intrinsic probe at the interface between pentamers allowed us to study the effect of changing the pH or adding GdnHCl using near-UV CD. Figure 4 shows that the near-UV CD signal at 280 nm disappears when the protein is incubated at pH 4.5. In the same way, the near-UV CD signal at 280 nm decays with the addition of 2.0*M* GdnHCl (see Fig. 4). These results altogether indicate a loss of asymmetric environment around Trp 127 when the protein dissociates into pentamers. It is important to notice that the loss of signal at 280 nm was not accompanied with a significant loss in the content of secondary structure (see Fig. 4, inset). This result constitutes another experimental proof of the existence of pentameric folded intermediates.

Subsequently, we analyzed the near-UV CD and the intrinsic Trp fluorescence signals obtained for BLS-W22A-F127W incubated with increasing concentration of GdnHCl [Fig. 5(A)]. As can be seen using both techniques, the introduced probe is able to sense the intermediate species induced by chemical agents. Both curves almost perfectly overlap and show the dissociation equilibrium between 1.5 and 2.2*M* GdnHCl corresponding to the decamer–pentamer equilibrium previously reported for the wild-type protein by means of SLS. After a valley at around 2.2–2.5*M* GdnHCl, a second equilibrium between 2.5 and 3.0*M* GdnHCl detects the dissociation and unfolding of pentamers into monomers as previously described. Thus, the dissociation of the decamers into pentamers becomes evident using these spectroscopic techniques. In contrast, the FT spectra of the BLS-W22A-

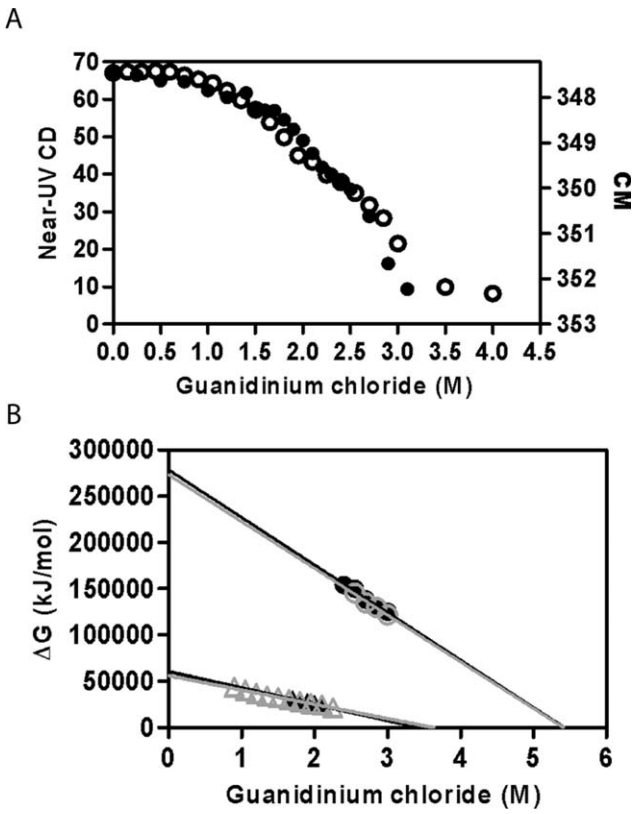

Figure 5

Dissociation and unfolding of BLS-W22A-F127W followed by fluorescence and near-UV CD. **A:** The samples (10 μ*M* of monomers) were incubated in 50 m*M* sodium phosphate, pH 7.0, containing different amounts of GdnHCl. After 2 h of incubation at room temperature, the following parameters were measured: molar ellipticity at 280 nm ([θ] (deg cm^2 dmol^{-1}) by near-UV CD (●) and center of mass by fluorescence (○). **B:** Linear extrapolation of Δ*G*1 and Δ*G*2 values for BLS-W22A-F130W. Δ*G*1 measured by near-UV CD (▲) and fluorescence (Δ) and Δ*G*2 measured by far-UV CD (●) and fluorescence (○).

Table I
Thermodynamic Parameters

	BLS	BLS-W22A-F130W
	Dissociation ($\Delta G1$) (kJ/mol)	
SLS	90 ± 20	n.d.
DLS	98 ± 15	89 ± 36
FT	n.d.	56 ± 2
Near-UV CD	n.d.	63 ± 4
	Unfolding ($\Delta G2$) (kJ/mol)	
FT	296 ± 58	309 ± 41
Far-UV CD	320 ± 22	343 ± 25
ΔG total (kJ/mol)	401 ± 57	396 ± 47

$\Delta G1$ (kJ/mol of monomer) of BLS and BLS-W22A-F127W was calculated from dynamic light scattering, fluorescence and near-UV CD spectra analysis. $\Delta G2$ (kJ/mol of monomer) of BLS and BLS-W22A-F127W was calculated from fluorescence and far-UV CD spectra analysis. The total ΔG value for each protein was calculated by an average of the $\Delta G1$ and $\Delta G2$ values obtained from different techniques.

F121W does not show clear two-state dissociation equilibrium (data not shown), reinforcing the selection of the BLS-W22A-F127W mutant described at the end of the previous section for further studies.

The analysis of the dissociation of the decamer into pentamers using SLS[11] and DLS (this work) shows a very similar $\Delta G1$ for the WT and the mutant (~90 kJ/mol, Table I). As Figure 5(B) shows, the regression analysis for this equilibrium determined by FT and near-UV CD using the introduced probe in the mutant shows a marked decrease of about 30% in this parameter (see also Table I for comparison). This fact could be due to the different protein concentrations used or to the different sensitivity of the techniques applied. A larger sensitivity of the spectroscopic techniques should allow sensing some disturbing effects of the bulky Trp residues introduced at the pentamer–pentamer interface.

On the other hand, the transition from a folded pentamer to unfolded monomers both in the WT and the mutant is a highly cooperative process that occurs at higher concentrations of GdnHCl. In both cases, the equilibrium could be measured by Trp fluorescence and far-UV CD. In the case of the mutant, analysis by near-UV CD shows similar results (Table I). All the applied spectroscopic techniques show a sharp and overlapping change around 2.4–3.5*M* GdnHCl, ruling out the existence of a populated intermediate during this transition. In summary, the thermodynamic analysis of this equilibrium shows that the $\Delta G2$ is very similar, indicating that the mutation does not alter the monomer–monomer interface at a large extent. Finally, the ΔG_{total} values of the wild type and the mutant calculated using parameters obtained by a combination of techniques (Table I) show that the overall stability of the protein is not altered by the introduction of the probe.

Thermal denaturation analysis of the wild-type protein monitored by far-UV CD showed a sharp and irreversible transition at a very high temperature (88°C), sensing the loss in secondary structure associated with the dissociation and unfolding of the pentamers (equilibrium 2, see Zylberman et al.[11]). The introduced probe allowed us to follow the thermal denaturation of the mutant by near-UV CD signal. As the introduced asymmetric Trp responsible for this signal is located at the pentamer–pentamer interface, we were able to sense the dissociation of the decamer into pentamers by applying heat to the sample (see Fig. 6). This equilibrium takes place between 55 and 70°C and is cooperative and reversible, and the protein then irreversibly denaturates and aggregates at around 80°C. The possibility of reversible dissociate of the pentamers by heating can be used for vaccine and protein-engineering purposes,[12] as BLS can be decorated with different antigens controlling the geometry and stoichiometry (mixed chimeras).

Conclusions

The decoration of homooligomeric scaffolds for biotechnological applications is a field of increasing interest. BLS is an example of this trend.[12,13,15,16,30] Controlling the assembly of the particles could be very important for several reasons, for example, when the geometry or density of the decorating chemical entity is important in vivo for functional reasons. In this work, we show that the rational introduction of an intrinsic Trp probe allowed us to efficiently measure and control the dissociation of a decamer into the composing pentamers. This simple procedure can be applied to other proteins of biotechnological interest that form particles. Exchanging

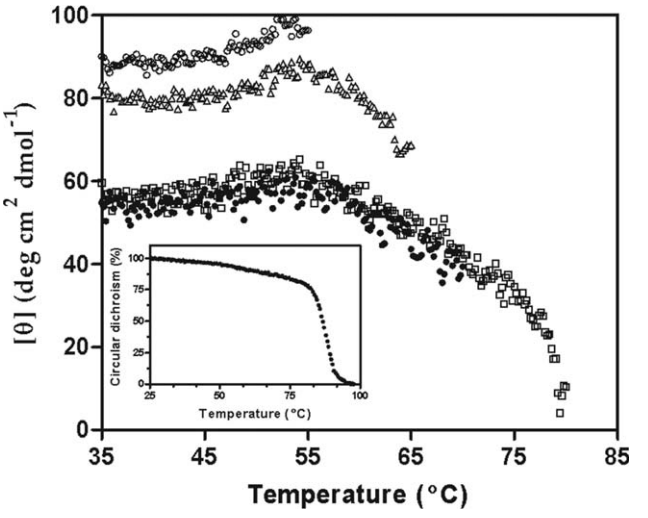

Figure 6
Analysis of the reversibility of thermal denaturation followed by near-UV CD. The thermal denaturation of BLS-W22A-F127W was followed by circular dichroism at 280 nm. The protein at a concentration of 1.4 mg/mL was first heat until 55°C (○). After cooling for 1 h at room temperature, the sample was then heated until 65°C (Δ) and cooled again. This process was repeated twice reaching 70°C (●) and 80°C (□). Inset: The thermal denaturation followed by far-UV CD is shown.

bulky Phe or Tyr residues at protein interfaces for Trp can be an efficient way to introduce these probes, if the overall stability of the particle is not compromised by the structural change.

REFERENCES

1. Ladenstein R, Schneider M, Huber R, Bartunik HD, Wilson K, Schott K, Bacher A. Heavy riboflavin synthase from *Bacillus subtilis*. Crystal structure analysis of the icosahedral beta 60 capsid at 3.3 A resolution. J Mol Biol 1988;203:1045–1070.
2. Neuberger G, Bacher A. Biosynthesis of riboflavin. Enzymatic formation of 6,7-dimethyl-8-ribityllumazine by heavy riboflavin synthase from *Bacillus subtilis*. Biochem Biophys Res Commun 1986;139:1111–1116.
3. Volk R, Bacher A. Biosynthesis of riboflavin. Studies on the mechanism of L-3,4-dihydroxy-2-butanone 4-phosphate synthase. J Biol Chem 1991;266:20610–20618.
4. Volk R, Bacher A. Studies on the 4-carbon precursor in the biosynthesis of riboflavin. Purification and properties of L-3,4-dihydroxy-2-butanone-4-phosphate synthase. J Biol Chem 1990;265:19479–19485.
5. Persson K, Schneider G, Jordan DB, Viitanen PV, Sandalova T. Crystal structure analysis of a pentameric fungal and an icosahedral plant lumazine synthase reveals the structural basis for differences in assembly. Protein Sci 1999;8:2355–2365.
6. Morgunova E, Meining W, Illarionov B, Haase I, Jin G, Bacher A, Cushman M, Fischer M, Ladenstein R. Crystal structure of lumazine synthase from *Mycobacterium tuberculosis* as a target for rational drug design: binding mode of a new class of purinetrione inhibitors. Biochemistry 2005;44:2746–2758.
7. Gerhardt S, Haase I, Steinbacher S, Kaiser JT, Cushman M, Bacher A, Huber R, Fischer M. The structural basis of riboflavin binding to *Schizosaccharomyces* pombe 6,7-dimethyl-8-ribityllumazine synthase. J Mol Biol 2002;318:1317–1329.
8. Zhang X, Meining W, Cushman M, Haase I, Fischer M, Bacher A, Ladenstein R. A structure-based model of the reaction catalyzed by lumazine synthase from *Aquifex aeolicus*. J Mol Biol 2003;328:167–182.
9. Zhang X, Meining W, Fischer M, Bacher A, Ladenstein R. X-ray structure analysis and crystallographic refinement of lumazine synthase from the hyperthermophile *Aquifex aeolicus* at 1.6 A resolution: determinants of thermostability revealed from structural comparisons. J Mol Biol 2001;306:1099–1114.
10. Ritsert K, Huber R, Turk D, Ladenstein R, Schmidt-Base K, Bacher A. Studies on the lumazine synthase/riboflavin synthase complex of *Bacillus subtilis*: crystal structure analysis of reconstituted, icosahedral beta-subunit capsids with bound substrate analogue inhibitor at 2.4 A resolution. J Mol Biol 1995;253:151–167.
11. Zylberman V, Craig PO, Klinke S, Braden BC, Cauerhff A, Goldbaum FA. High order quaternary arrangement confers increased structural stability to Brucella sp. lumazine synthase. J Biol Chem 2004;279:8093–8101.
12. Laplagne DA, Zylberman V, Ainciart N, Steward MW, Sciutto E, Fossati CA, Goldbaum FA. Engineering of a polymeric bacterial protein as a scaffold for the multiple display of peptides. Proteins 2004;57:820–828.
13. Rosas G, Fragoso G, Ainciart N, Esquivel-Guadarrama F, Santana A, Bobes RJ, Ramirez-Pliego O, Toledo A, Cruz-Revilla C, Meneses G, Berguer P, Goldbaum FA, Sciutto E. Brucella spp. lumazine synthase: a novel adjuvant and antigen delivery system to effectively induce oral immunity. Microbes Infect 2006;8:1277–1286.
14. Sciutto E, Toledo A, Cruz C, Rosas G, Meneses G, Laplagne D, Ainciart N, Cervantes J, Fragoso G, Goldbaum FA. Brucella spp. lumazine synthase: a novel antigen delivery system. Vaccine 2005;23:2784–2790.
15. Bellido D, Craig PO, Mozgovoj MV, Gonzalez DD, Wigdorovitz A, Goldbaum FA, Dus Santos MJ. Brucella spp. lumazine synthase as a bovine rotavirus antigen delivery system. Vaccine 2009;27:136–145.
16. Craig PO, Berguer PM, Ainciart N, Zylberman V, Thomas MG, Martinez Tosar LJ, Bulloj A, Boccaccio GL, Goldbaum FA. Multiple display of a protein domain on a bacterial polymeric scaffold. Proteins 2005;61:1089–1100.
17. Estein SM, Fiorentino MA, Paolicchi FA, Clausse M, Manazza J, Cassataro J, Giambartolomei GH, Coria LM, Zylberman V, Fossati CA, Kjeken R, Goldbaum FA. The polymeric antigen BLSOmp31 confers protection against *Brucella ovis* infection in rams. Vaccine 2009;27:6704–6711.
18. Cruz-Revilla C, Toledo A, Rosas G, Huerta M, Flores-Perez I, Pena N, Morales J, Cisneros-Quinones J, Meneses G, Diaz-Orea A, Anciart N, Goldbaum F, Aluja A, Larralde C, Fragoso G, Sciutto E. Effective protection against experimental *Taenia solium* tapeworm infection in hamsters by primo-infection and by vaccination with recombinant or synthetic heterologous antigens. J Parasitol 2006;92:864–867.
19. Jelesarov I, Karshikoff A. Defining the role of salt bridges in protein stability. Methods Mol Biol 2009;490:227–260.
20. Mohan PM, Hosur RV. pH dependent unfolding characteristics of DLC8 dimer: Residue level details from NMR. Biochim Biophys Acta 2008;1784:1795–1803.
21. Tettamanzi MC, Keeler C, Meshack S, Hodsdon ME. Analysis of site-specific histidine protonation in human prolactin. Biochemistry 2008;47:8638–8647.
22. Klinke S, Zylberman V, Vega DR, Guimaraes BG, Braden BC, Goldbaum FA. Crystallographic studies on decameric Brucella spp. Lumazine synthase: a novel quaternary arrangement evolved for a new function? J Mol Biol 2005;353:124–137.
23. Klinke S, Zylberman V, Bonomi HR, Haase I, Guimaraes BG, Braden BC, Bacher A, Fischer M, Goldbaum FA. Structural and kinetic properties of lumazine synthase isoenzymes in the order Rhizobiales. J Mol Biol 2007;373:664–680.
24. Sobolev V, Sorokine A, Prilusky J, Abola EE, Edelman M. Automated analysis of interatomic contacts in proteins. Bioinformatics 1999;15:327–332.
25. McGaughey GB, Gagne M, Rappe AK. pi-Stacking interactions. Alive and well in proteins. J Biol Chem 1998;273:15458–15463.
26. Dundas J, Ouyang Z, Tseng J, Binkowski A, Turpaz Y, Liang J. CASTp: computed atlas of surface topography of proteins with structural and topographical mapping of functionally annotated residues. Nucleic Acids Res 2006;34(Web Server issue):W116–W118.
27. Goldbaum FA, Velikovsky CA, Baldi PC, Mortl S, Bacher A, Fossati CA. The 18-kDa cytoplasmic protein of Brucella species—an antigen useful for diagnosis–is a lumazine synthase. J Med Microbiol 1999;48:833–839.
28. Kammann M, Laufs J, Schell J, Gronenborn B. Rapid insertional mutagenesis of DNA by polymerase chain reaction (PCR). Nucleic Acids Res 1989;17:5404.
29. Vuilleumier S, Sancho J, Loewenthal R, Fersht AR. Circular dichroism studies of barnase and its mutants: characterization of the contribution of aromatic side chains. Biochemistry 1993;32:10303–10313.
30. Cassataro J, Pasquevich KA, Estein SM, Laplagne DA, Velikovsky CA, de la Barrera S, Bowden R, Fossati CA, Giambartolomei GH, Goldbaum FA. A recombinant subunit vaccine based on the insertion of 27 amino acids from Omp31 to the N-terminus of BLS induced a similar degree of protection against B. ovis than Rev. 1 vaccination. Vaccine 2007;25:4437–4446.
31. Greene RF, Jr, Pace CN. Urea and guanidine hydrochloride denaturation of ribonuclease, lysozyme, α-chymotrypsin, and β-lactoglobulin. J Biol Chem 1974;249:5388–5393.

APPENDIX

The equilibrium constant $K_{U(2)}$ and the free energy change $\Delta G_{U(2)}$ for this transition are defined in Eqs. (8) and (9).

$$K_{U(2)} = [U]^2/[N_5] \tag{8}$$

$$\Delta G_{U(2)} = -RT \ln K_{U(2)} \tag{9}$$

The total protein concentration in monomer units (P_T) and the fractional population in the native (F_N) and unfolded (F_U) states were calculated using Eqs. (10–12),

$$P_T = 5[N_5] + [U] \quad (10)$$

$$F_N = 5[N_5]/P_T \quad (11)$$

$$F_U = 1 - F_N = [U]/P_T = (m_f[D] + F) - Y/[(m_f[D] + F) - (m_u[D] - U)] \quad (12)$$

where Y is the experimental spectroscopic value, $[D]$ is the GdnHCl concentration, F and U are the intercepts, and m_f and m_u are the slopes of the pre- and postunfolding baselines, respectively. Combining Eqs. (1) and (8–12), we obtain the general equation [Eq. (13)].